



Cite this: *Soft Matter*, 2017,  
13, 600

Received 5th October 2016,  
Accepted 12th December 2016

DOI: 10.1039/c6sm02259f

[www.rsc.org/softmatter](http://www.rsc.org/softmatter)

## DNA packaging in viral capsids with peptide arms

Qianqian Cao<sup>\*abc</sup> and Michael Bachmann<sup>bde</sup>

Strong chain rigidity and electrostatic self-repulsion of packed double-stranded DNA in viruses require a molecular motor to pull the DNA into the capsid. However, what is the role of electrostatic interactions between different charged components in the packaging process? Though various theories and computer simulation models were developed for the understanding of viral assembly and packaging dynamics of the genome, long-range electrostatic interactions and capsid structure have typically been neglected or oversimplified. By means of molecular dynamics simulations, we explore the effects of electrostatic interactions on the packaging dynamics of DNA based on a coarse-grained DNA and capsid model by explicitly including peptide arms (PAs), linked to the inner surface of the capsid, and counterions. Our results indicate that the electrostatic interactions between PAs, DNA, and counterions have a significant influence on the packaging dynamics. We also find that the packed DNA conformations are largely affected by the structure of the PA layer, but the packaging rate is insensitive to the layer structure.

### Introduction

It is an important subject to investigate confinement dynamics of genomic double-stranded (ds) DNA in viral capsids with a diameter smaller than or comparable to the dsDNA persistence length.<sup>1–5</sup> Clearly, to accommodate within such a confined environment a dsDNA chain with a contour length hundreds of times larger than the capsid diameter is subject to high energetic and entropic penalties. Thus the polyelectrolyte is forced to form energetically unfavorable conformations. The packaging process is driven by a powerful molecular motor and the DNA is compressed into an almost crystalline state. As a result, tightly packed DNA exerts a high pressure onto the capsid shell. The internal force is necessary for the injection of the viral DNA into a host cell. Significant advancements in experimental techniques, such as single-molecule cryo-electron microscopy (cryo-EM)<sup>6,7</sup> and optical-tweezer techniques,<sup>1,8</sup> largely improve our understanding of the process dynamics (packaging and ejection) and the genome organization in the capsid interior.

However, there are still considerable difficulties in accurately identifying the morphologies of encapsulated genomes on

atomic and molecular scales. For example, cryo-EM images cannot provide information about the conformation of single DNA molecules, but rather the average distribution of the DNA density. Additionally, the conformation of packed dsDNA largely depends on the capsid structure and the ionic environment. The structural ordering of the genomes in some typical bacteriophages such as T7,  $\phi$ 29, and  $\lambda$ , is not universal, but some conformational features are rather unique. Structural differences potentially cause large discrepancies in ejection forces and packaging dynamics.<sup>9</sup> It is fair to say that the packaging process of the viral genome and its conformational properties in the preassembled capsid are not completely understood.

The protein hull of a capsid contains under physiological conditions positively charged peptide arms (PAs), which extend into the interior of the capsid. Theoretical studies have investigated the electrostatic properties of the PAs and the genome as well as the radial density of the genome.<sup>10,11</sup> Based on self-consistent field (SCF) theory and experimental data analysis, it was shown that nonspecific electrostatic interactions dominate in a subclass of ssRNA viruses and control both the amount of encapsulated ssRNA and its density distribution.<sup>10</sup> The theory predicted a charge ratio of 1.8, close to the best-fit experimental value 1.6. However, other studies indicated that a specific charge ratio between the packed genome and the capsid does not exist, and the ratio is sensitive to the set of viruses which were chosen for the analysis.<sup>11</sup> To this end, it is still not clear how the structural features and charge distribution of PAs, such as arm length and density, affect the genome packaging dynamics and the degree of conformational order.

Previous theoretical and simulational studies,<sup>2,9,10,12–23</sup> aiming at conformational and dynamic properties of DNA packaging,

<sup>a</sup> College of Mechanical and Electrical Engineering, Jiaxing University, Jiaxing 314001, P. R. China. E-mail: qqcao@mail.zjxu.edu.cn

<sup>b</sup> Soft Matter Systems Research Group, Center for Simulational Physics, The University of Georgia, Athens, GA 30602, USA. E-mail: bachmann@smsyslab.org; Web: <http://www.smsyslab.org>

<sup>c</sup> Institut für Theoretische Physik, Freie Universität Berlin, Arnimallee 14, 14195 Berlin, Germany

<sup>d</sup> Instituto de Física, Universidade Federal de Mato Grosso, Cuiabá (MT), Brazil

<sup>e</sup> Departamento de Física, Universidade Federal de Minas Gerais, Belo Horizonte (MG), Brazil

were based on simple models for the internal structure of the capsid and electrostatic features of DNA–DNA and DNA–capsid interactions. Most computational models neglect the electrostatic interaction or only consider it as a potential of mean force based on Debye–Hückel theory. Many details of viral capsids, which are generally modeled as spheres or geometries composed of trigonal subunits with bare surfaces, are also ignored. To what extent these simplified model assumptions impact the packaging and ejection dynamics as well as the structure of the enclosed genome is still unknown. Molecular dynamics simulations of all-atom models<sup>24</sup> are typically limited to nanosecond time-scales, whereas packaging of realistic systems takes considerably longer. Furthermore, the release and accumulation of counterions in the capsid influences the packaging dynamics as well. However, this effect cannot be captured by implicit-ion models. Therefore, explicitly including ions in viral models is necessary in certain cases such as in the low salt concentration limit or for multivalent salt. Recently, optical-tweezer experiments on  $\phi$ 29 under different ionic conditions revealed that the effects of ionic screening can strongly affect the physics of dsDNA confinement and the function of the ATP-driven motor.<sup>8</sup> High-valent ions that can effectively screen the DNA charge and even induce DNA condensation in high ion concentrations lead to a reduced internal pressure. However, there is no simple relationship between packaging rate and ionic screening because of the ionic effects on the motor function.

In this work, a coarse-grained (CG) model was employed to mimic the dsDNA chain and the capsid. In the generic semi-flexible DNA model we used, the helical structure of DNA was ignored, because the length scale of secondary structures is smaller than the persistence length of the chain, which is most relevant for the packaging properties of the DNA chain. In ref. 25, a phenomenological cholesteric twist potential was taken into account to address details of the interplay of the helical structure of DNA and the interaction between the effective charges of the double-helical molecule. However, it is still not completely clear how the helical structure of dsDNA influences the packaging dynamics of the DNA chain. For our study of DNA packaging dynamics, we explicitly took into account internal PAs and counterions. Conformations of packed DNA depend on the structural characteristics of charged PAs, the shape of the capsid, and DNA elasticity. Moreover, the packaging process is also largely influenced by the effective capsid charges, especially if motor forces are weak and PAs dense. The electrostatic attraction between the DNA and PAs can partly counterbalance an increase in the DNA bending and intra-DNA electrostatic repulsion, which can accelerate the DNA intrusion.

## Model and method details

The dsDNA chain in our CG model consists of  $N_d = 600$  spherical beads (monomers) of diameter  $\sigma_{dd} + \Delta_{dd} = 25 \text{ \AA}$ , where  $\sigma_{dd} = 11 \text{ \AA}$  and  $\Delta_{dd} = 14 \text{ \AA}$  are model parameters we introduce below ( $\sigma_{dd}$  is chosen as the unit for length scales). Each DNA bead represents about  $N_b = 3.75$  base pairs. The capsid that is simulated as a sphere with radius  $R = 14\sigma_{dd}$  includes 4195 frozen beads, and possesses an open cylindrical channel of radius  $R_{in} = 1.6\sigma_{dd}$  and

length  $L_{in} = 2\sigma_{dd}$ . The DNA chain can be fed through this channel into the cavity by a portal motor which for real viruses has a complex structure. To capture a DNA bead and pull it into the capsid, we apply a radial force  $f$  to the bead once it enters the opening. The magnitude of the applied force is chosen between 0 and  $200f^*$ , where  $f^* = k_B T / \sigma_{dd}$  is the force unit. In the absence of motor force, a polymer chain can intrude into the cavity only spontaneously by electrostatic interactions between monomers and surface charges.<sup>26</sup> The details of the force-driven mechanism do not influence the packaging dynamics.

$N_p$  flexible PAs with  $N_{pm}$  beads per chain are densely grafted on the inner surface of the capsid and resemble polyelectrolyte brushes.<sup>10</sup> The grafting density investigated here ranges from  $\rho_g = N_p / (4\pi R^2) = 0.0138\sigma_{dd}^{-2}$  ( $N_p = 34$ ) to  $0.305\sigma_{dd}^{-2}$  (750), entailing a spacing of 19.9  $\text{\AA}$  to 93.6  $\text{\AA}$  between each other. We only consider the net charge distribution in each PA with charge fraction 0.5, *i.e.*, 2 neighboring beads share one unit of positive charge. In the PA model, each bead represents an amino acid unit. The initial system configuration is illustrated in Fig. 1 (counterions are not shown).

The potential energy of the system can be divided into four contributions: short-range van der Waals effects ( $U_{LJ}$ ), chain connectivity constraint ( $U_{bond}$ ), bending rigidity ( $U_{angle}$ ), and long-range Coulomb interaction ( $U_e$ ). Van der Waals interactions and excluded volume are modeled by the expanded Lennard-Jones (LJ) potential

$$U_{LJ}^{\alpha\beta}(r) = 4\epsilon_{\alpha\beta} \left[ \left( \frac{\sigma_{\alpha\beta}}{r - \Delta_{\alpha\beta}} \right)^{12} - \left( \frac{\sigma_{\alpha\beta}}{r - \Delta_{\alpha\beta}} \right)^6 + \frac{1}{4} \right], \quad (1)$$

where  $\alpha$  and  $\beta$  denote DNA (d) and PA (p) monomers, or Na (n) and Cl (c) counterions. The LJ potential is truncated and shifted at a cutoff distance of  $r_c = \Delta_{\alpha\beta} + 2^{1/6}\sigma_{\alpha\beta}$ . In addition to  $\Delta_{dd}$  and  $\sigma_{dd}$  we set  $\Delta_{pp} = 0$  and  $\sigma_{pp} = 7.5 \text{ \AA}$ ;  $\Delta_{nn} = \Delta_{cc} = 0$  and  $\sigma_{nn} = \sigma_{cc} = 4 \text{ \AA}$  (regardless of ion-specific effects). The potential strength  $\epsilon_{\alpha\beta}$  is set to  $1k_B T$  for all energetic components. The system temperature is  $T = 300 \text{ K}$ . We employ the Lorentz–Berthelot mixing rule to

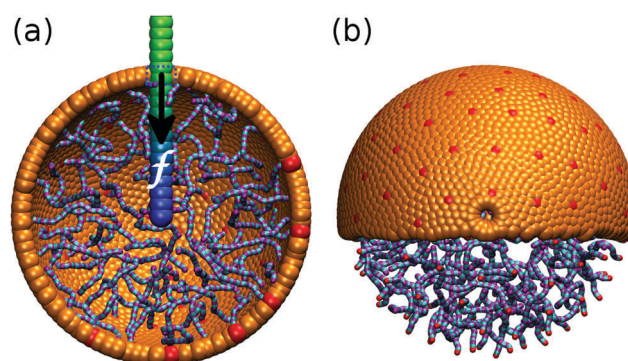


Fig. 1 Schematic representation of the model system. One end of the dsDNA chain is located inside the portal region, pointing into the capsid. The packaging process is driven by the electrostatic attraction between the DNA and PAs as well as by the motor force  $f$ . Cross sections of the capsid are shown from the (a) side and (b) top. Counterions are not shown. Color scheme: capsid (orange), grafted beads (red), charged (purple) and neutral (cyan) peptide units, DNA chain (colored with a RGB scheme).

calculate the LJ parameters for dissimilar particles. The modified form of the LJ potential is particularly useful to model systems with particles of different sizes such as DNA-grafted colloids.<sup>27</sup> Steric interactions between components  $\alpha$  and  $\beta$  diverge at the separation  $A_{\alpha\beta}$  rather than at zero distance as in the standard LJ potential.

The elasticity of bonds in the DNA and PA chains is described by the harmonic bond potential

$$U_{\text{bond}}(b) = \frac{k_b}{2}(b - b_0)^2, \quad (2)$$

where the equilibrium bond length  $b_0$  for the DNA chain is  $(\sigma_{\text{dd}} + A_{\text{dd}})/2$  and  $\sigma_{\text{pp}}/2$  for the PA. The spring constant of the DNA chain is set to  $56 \text{ kJ mol}^{-1} \text{ \AA}^{-2}$  through  $k_b = k_{\text{bp}}/N_b$  where  $k_{\text{bp}} = 210 \text{ kJ mol}^{-1} \text{ \AA}^{-2}$  is the spring constant of B-DNA for one base pair length. The length of a virtual bond between amino acid residues in the PA is kept constant. To mimic a ropelike, cylindrical chain model, the bead size is set to twice the bond length. Moreover, the pair interactions (including LJ and Coulomb potentials) between overlapping bonded monomers are not considered. The semiflexibility of the DNA chain is taken into account by the harmonic potential

$$U_{\text{angle}}(\theta) = \frac{k_\theta}{2}(\theta - \theta_0)^2, \quad (3)$$

where  $\theta$  is the angle between successive bonds and the reference angle  $\theta_0$  is set to  $\pi$ . From the wormlike-chain model, the bending rigidity of DNA is obtained as  $k_\theta = k_B T l_p / b_0 \approx 40 k_B T \text{ rad}^{-2}$ , where we used  $l_p \approx 500 \text{ \AA}$  as the static persistence length of DNA at physiological conditions. The PAs are considered fully flexible ( $k_\theta = 0$ ).<sup>28</sup>

The long-range electrostatic interaction is modeled by the Coulomb potential

$$U_c^{\alpha\beta}(r) = k_B T Z_\alpha Z_\beta \frac{\lambda_B}{r}, \quad (4)$$

where  $Z_\alpha$  is the charge valence of the  $\alpha$  component. We chose bare charge values  $Z_d = 7.5$  for each DNA bead and  $Z_p = 1$  for a charged peptide bead. As the counterions of the 600 DNA monomers, 4500 Na ions were used. The number of Cl ions as PA counterions depends on PA grafting densities and arm lengths, which were varied in our comparative study. The Bjerrum length  $\lambda_B = e^2 / (4\pi\epsilon_0\epsilon_r k_B T)$ , where  $\epsilon_0$  and  $\epsilon_r$  are the vacuum permittivity and the dielectric constant of the solvent, respectively, is  $7.1 \text{ \AA}$  for water at room temperature. The long-range part of the Coulomb interaction is calculated by means of the particle-particle/particle-mesh (P3M) algorithm.<sup>29</sup>

We employed LAMMPS<sup>30</sup> to perform Langevin thermostated molecular dynamics simulations in a periodic cubic simulation box of edge length  $800\sigma_{\text{dd}}$ . The coupling time constant in the Langevin thermostat was  $\tau = 3.34 \text{ ps}$  and the time step  $\Delta t = 26.7 \text{ fs}$ . The longest trajectory we simulated was about  $5 \text{ ms}$ , which corresponds to approximately  $5.6 \times 10^7$  time steps.

## Results and discussion

The packaging amount of DNA and counterions is defined as the number of respective particles (DNA beads or counterions)

located inside the capsid. Fig. 2 shows this quantity as a function of simulation time for two cases,  $N_p = 150$  ( $N_{\text{pm}} = 30$ ) and  $N_p = 750$  ( $N_{\text{pm}} = 6$ ). The total number of PA charged units remains constant at 2250. It was found that the PA counterions are released off the capsid as the packaging amount of DNA increases. After all PA counterions are depleted, the DNA counterions begin to diffuse into the cavity, *i.e.*, DNA and PA counterions are rarely present at the same time in the capsid (see also snapshots in Fig. 2). The dynamic behavior of counterion release or accumulation can neither be captured by bead-spring polymer models nor CG models of DNA based on the Debye-Hückel (DH) approximation, especially in the low salt concentration limit. MD simulations indicated that the number of counterions in a neutral spherical cavity is much lower than the bare charge of the packed polyelectrolyte chain, and that it is independent of the concentration of monovalent salt.<sup>31</sup> Therefore, using the DH approximation based on the bulk salt concentration outside the capsid may have a great influence on the packaging dynamics.

In the initial phase of the packaging process, the number of PA counterions in the capsid is smaller for  $N_p = 750$  than for  $N_p = 150$ .

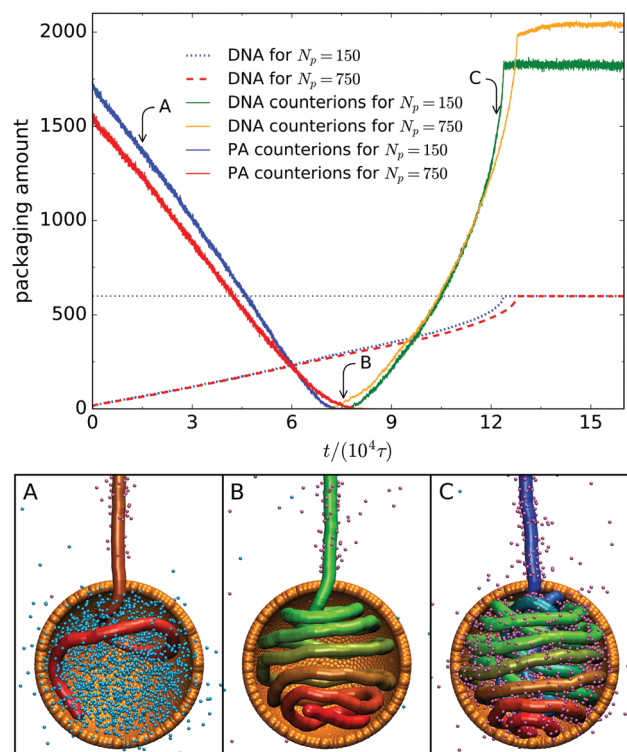


Fig. 2 Top panel: Time evolution of the packaging amount for the DNA chain and counterions at  $N_p = 150$  ( $N_{\text{pm}} = 30$ ) and  $N_p = 750$  ( $N_{\text{pm}} = 6$ ). Bottom panel: Snapshots for  $N_p = 150$  corresponding to A–C in the top panel. Small cyan and mauve beads represent DNA counterions and PA counterions, respectively. The constant total number of PA charged units is 2250. The applied motor force during packaging is  $100f^*$ . The DNA chain is depicted as a cylindrical pipeline colored with a RGB scheme (red  $\rightarrow$  green  $\rightarrow$  blue) for visual clarity (the red segment is the head one that initially enters the portal motor). The PAs are not shown in the snapshots. Note that the amount of packed DNA segments corresponds to the number  $N_b$  of coarse-grained DNA beads, *i.e.*, base pairs.

After the packaging process is finished, more DNA counterions remain in the capsid for  $N_p = 750$ . The packaging amount of DNA does not show an observable difference for both cases. Close to the end the DNA chain is packaged slightly more rapidly for  $N_p = 150$ .

Typical conformations of packed DNA and charge densities of DNA, PA, and their counterions for different PA lengths are shown in Fig. 3. The interaction between the DNA chain and the capsid is described by the expanded LJ potential given by eqn (1). Therefore, the width of the depletion region between the center of the DNA beads and the capsid surface can be approximately estimated as  $(\Delta_{dd} + \sigma_{dd} + \sigma_{pp})/2 = 1.48\sigma_{dd}$ . However, the PA chains are grafted to the capsid surface by harmonic bonds. The bond length is  $\sigma_{pp}/2 = 0.34\sigma_{dd}$ , which is much less than the width of this depletion zone. Moreover, the PA brush has little effect on the size of the depletion region because the excluded volume effect originating from the grafting density of the PA chains investigated in our simulations is not sufficiently strong to overwhelm the electrostatic attraction between the DNA and PA chains. The maximum peak of the DNA charge density increases with  $N_p$ . After DNA inclusion, virtually no PA counterions are found in the capsid. Conversely, the density of the DNA counterions outside the shell is also largely reduced. For sufficiently high PA density, *e.g.*, for  $N_p = 750$ , the DNA counterions confined inside the capsid do not intrude into the PA layer. While the packaging process of the DNA is

weakly influenced by the PA length, the morphology of the packed DNA conformation depends significantly on the PA length (see typical snapshots in Fig. 3). Compared to the DNA which forms layers, the DNA counterions distribute more uniformly inside the capsid.

To elucidate the correlation between the DNA and PA chains, we present the corresponding radial distribution function (RDF)  $g_{dp}(r)$  in Fig. 4. Though the total number of the PA beads is kept constant,  $g_{dp}(r)$  depends on the PA length and grafting density. For the shortest PA chains and densest grafting layer ( $N_{pm} = 6$  and  $N_p = 750$ ), the first peak becomes more pronounced compared to the other two cases. This can be attributed to the compact arrangement of the packed DNA close to the surface (see Fig. 3), which implies strong electrostatic correlation between the DNA and PA beads in the packed compound layer. As  $r$  increases,  $g_{dp}$  is remarkably reduced. Additionally, the correlation is enhanced for longer PA as they tend to extend into the interior of the capsid and to interact with the inner DNA layer.

Fig. 5 presents the packaging amount of DNA for various peptide arm configurations at the interior capsid surface,  $N_p$  and  $N_{pm}$ , with or without aid of motor force. First, we analyze the evolution of the packaging amount for the specific cases of  $N_p = 150$  and  $N_{pm} = 30$ . Not surprisingly, increasing the motor force leads to a faster packaging process. In the absence of motor force, the packaging amount increases linearly until the number of packed DNA charges compensates the PA charges (namely below the lower horizontal line in Fig. 5). Thereafter, the DNA continues to be packed into the capsid at a very slow speed. Finally, the packaging stops when the number of packed DNA monomers reaches approximately 350 after a long simulation  $t \approx 120 \times 10^4 \tau$  (about 4  $\mu\text{s}$ ,  $1.5 \times 10^8$  time steps). The long-time dynamics for this case is also shown in Fig. 8(a). The average charge ratio between the DNA and PAs is 1.17, which is smaller than 1.6 from experimental measurement or 1.8 from theoretical predictions for ssDNA or ssRNA.<sup>10</sup> Evidently, the strong bending rigidity results in the reduced value. In the presence of motor force,

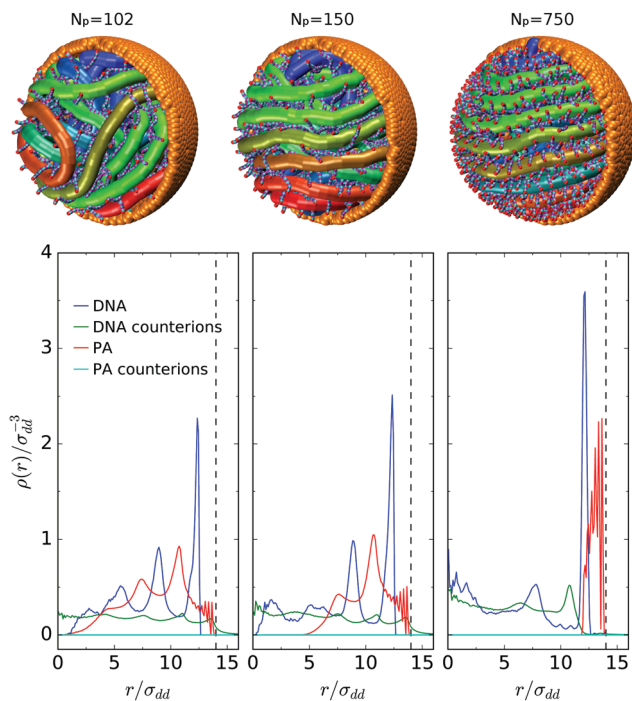


**Fig. 3** Top panel: Snapshots of the packed DNA chain in the capsid with PAs. Counterions are not shown. The color code of the capsid is the same as Fig. 1. The DNA chain is labeled with the color scheme in Fig. 2. Bottom panel: Radial charge densities of DNA, PAs and their counterions from the center of the capsid. Three cases from left to right correspond to  $N_p = 102$  ( $N_{pm} = 44$ ), 150 (30), and 750 (6), respectively. The motor force during packaging is  $100f^*$ . The vertical dotted line represents the position of the capsid hull.

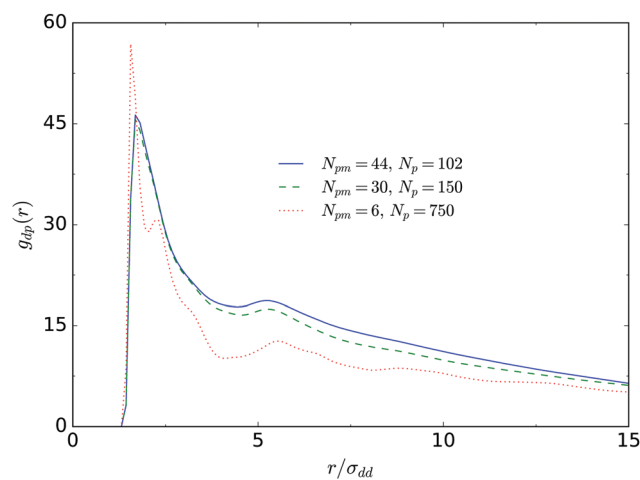


**Fig. 4** Radial distribution function between the DNA and PA beads for different  $N_{pm}$  and  $N_p$  at  $f/f^* = 100$ . These three cases correspond to those in Fig. 3.

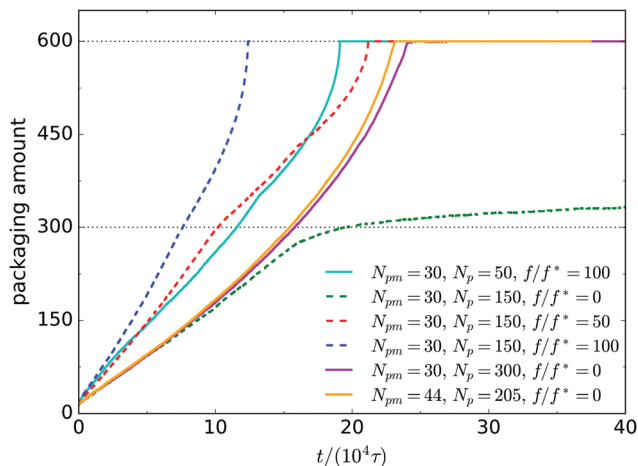


Fig. 5 Time evolution of the packaging amount of DNA with 600 monomers for various capsid models at different motor forces. The horizontal line at the top represents the maximum possible number of packed DNA beads. The lower line marks the amount of packed DNA, where the charge of which is equal to the total charge of PAs in the case of  $N_p = 150$  and  $N_{pm} = 30$ . Note that the system of  $N_p = 300$  and  $N_{pm} = 30$  includes approximately the same number of charged PA units as that of  $N_p = 205$  and  $N_{pm} = 44$ .

the intrusion is accelerated, and then the entire DNA enters the capsid.

For higher grafting density, such as  $N_p = 300$ , the inclusion process can still be completed on the simulation time scale though no motor force is applied on the DNA chain. It was found that the initial packaging rate is not biased in favor of the denser grafting. This indicates that in the absence of motor force the initial packaging rate is not dependent on the number of total charges in the PA layer, at least when changing  $N_p$  from 150 to 300. We also simulated the case with  $N_p = 205$  and  $N_{pm} = 44$  with approximately the same number of PA charges as for  $N_p = 300$  and  $N_{pm} = 30$ . However, the packaging rate in the final stage is slightly higher for the former. Longer PAs favor the packaging of DNA. For much sparser grafting density,  $N_p = 50$ , the motor force can significantly promote the packaging process. Compared to the case of  $N_p = 150$ , the packaging rate is much higher for the larger  $N_p$  under the same motor force  $f = 100f^*$ . The packaging rate at  $N_p = 150$  and  $f = 50f^*$  decreases after the packaging amount of DNA exceeds 300, and becomes smaller than that at  $N_p = 50$  and  $f = 100f^*$ . After the charges in the PA layer are counterbalanced by the DNA charges, the motor force dominates the packaging process.

Thermodynamic analysis of MD simulations reveals that the force opposing packaging not only results from the DNA–DNA repulsion but also from the entropic penalty of DNA confinement.<sup>34</sup> Unlike previous models without the internal PA chains, the electrostatic interaction between the DNA and PA chains, which is the only driving force to pull the DNA into the capsid in the absence of the motor, dominates over the energetic and entropic penalties of the packed DNA at sufficiently high grafting densities. When the number of the PA charges are balanced by the charges of already packed DNA, the motor force must exceed the force from the electrostatic and entropic

contribution of the section of the DNA chain that has not yet been packed.

In the cases of  $N_{pm} = 30$  ( $N_p = 300$ ) and  $N_{pm} = 44$  ( $N_p = 205$ ), where the number of the PA charges is equal to the number of DNA charges, the packaging rate becomes larger as the intrusion of the DNA continues. In the initial stage, the packed DNA undergoes structural rearrangements close to the capsid surface due to confinement and electrostatic interactions. Moreover, the grafted PA chains also tend to pull the DNA towards the grafting sites. These effects slow down the packaging speed. After the inner capsid surface has been covered by DNA monomers, the constraints to the DNA positions owing to the PA chains are reduced and the inner DNA layers adopt less ordered conformations. As a consequence, the packaging rate is increased to some extent in the packaging process of DNA in the interior of the capsid. Additionally, the release rate of the PA counterions also increases as it is accompanied by the DNA packaging. For the cases that the number of the PA charges is smaller than the number of DNA charges, the motor force is required to assist in completing the packaging process. After the packed DNA charges have compensated the PA charges, the packaging rate diminishes in the absence of a motor ( $N_{pm} = 30$ ,  $N_p = 300$ ,  $f/f^* = 0$ ) or if the motor force is too small ( $N_{pm} = 30$ ,  $N_p = 300$ ,  $f/f^* = 50$ ). If the motor force is sufficiently large, such as in the case  $f/f^* = 100$ , the packaging rate does not decrease during the entire process.

It is worth noting that a predominant increase of the packaging rate for the very last portion of the DNA chain is due to the reduced entropic force of the dangling tail outside the capsid in the cases where the DNA can be packaged completely. As the DNA tail becomes short, the packaging dynamics is sped up significantly.<sup>33</sup> If the DNA chain is longer or the capsid is smaller, corresponding to a higher packaging fraction, the increase in steric repulsion from the chain segment already packed inside suppresses further DNA intrusion. Entropic pulling of the expelled chain can also accelerate the DNA ejection process if a small part of the chain is left in the capsid.<sup>25</sup>

In Fig. 5, we show results of the DNA packaging at different PA length and grafting density in presence and absence of the motor force. From a polyelectrolyte brush point of view, the chain length and grafting density are two crucial physical parameters responsible for specific characteristics in the conformation and interaction of polyelectrolyte brushes compared to the neutral counterparts. Therefore, we also examine the packaging amount of DNA as a function of the PA length and grafting density, independently. The results are shown in Fig. 6. Several cases are already plotted in Fig. 5. The effect of the PA length is studied at a fixed number,  $N_p = 150$ , of the PA chains. As the chains are shortened, the packaging rate is reduced significantly (Fig. 6(a)). At the shortest chain length,  $N_{pm} = 4$ , the intrusion of the DNA stops when the number of packed DNA beads reaches about 30. Clearly, at low charge of the PA layer, the DNA–PA attraction is not sufficient to overcome the DNA bending energy from its intrinsic rigidity and electrostatic repulsion. For longer PA chains, the packaging rate starts to diminish after the number of the PA charges is counterbalanced

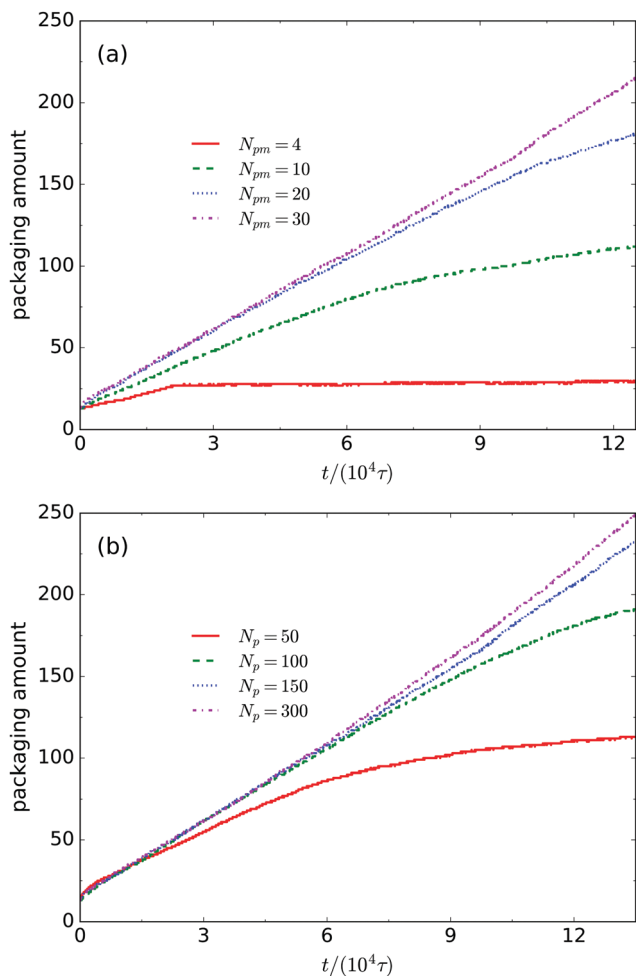


Fig. 6 Time evolution of the packaging amount of DNA with 600 monomers in the absence of motor force for (a) different length and (b) number (or grafting density) of the PA chains. In (a), the number of the PA chains is fixed at  $N_p = 150$ . In (b), the PA length is set to  $N_{pm} = 30$ .

by the DNA charges. Additionally, the point where the charges of the PA charges and that of the DNA charges are compensated each other is advanced at small  $N_{pm}$ . As the packaging process continues, the DNA chain is pulled into the capsid at a very slow rate until the equilibrium state is reached (not shown here). For  $N_{pm} = 30$ , a similar behavior on a large time scale is observed (Fig. 5). A smaller grafting density leads to a decreased packaging rate (Fig. 6(b)). However, we also find that unlike the variation of the chain length, the initial packaging rate is scarcely affected even at small number of the PA chains,  $N_p = 50$ , corresponding to the same number of the PA charges at the case of  $N_{pm} = 10$  in Fig. 6(a). By comparison, this again proves that the longer chains bring about a higher packaging rate at the same number of the PA charges.

It is evident from Fig. 7 that the radius of gyration  $R_g$  of the PA chains as a function of the number of the PA chains is proportional to the grafting density.  $R_g$  is calculated after the DNA chain is completely packed into the capsid. At low grafting densities, we exert a force of  $100f^*$  on the DNA chain to accomplish the packaging process, whereas no force is applied

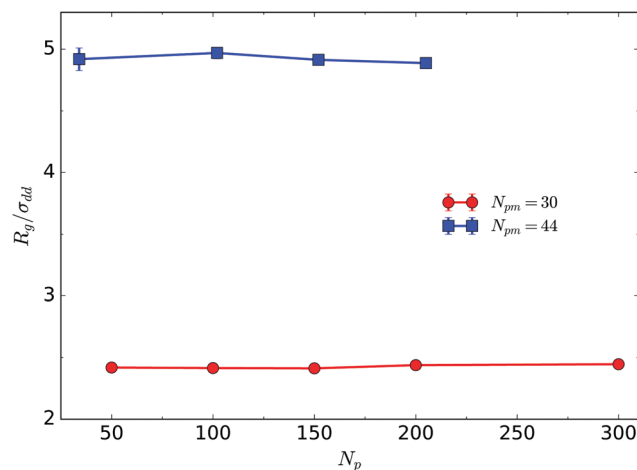
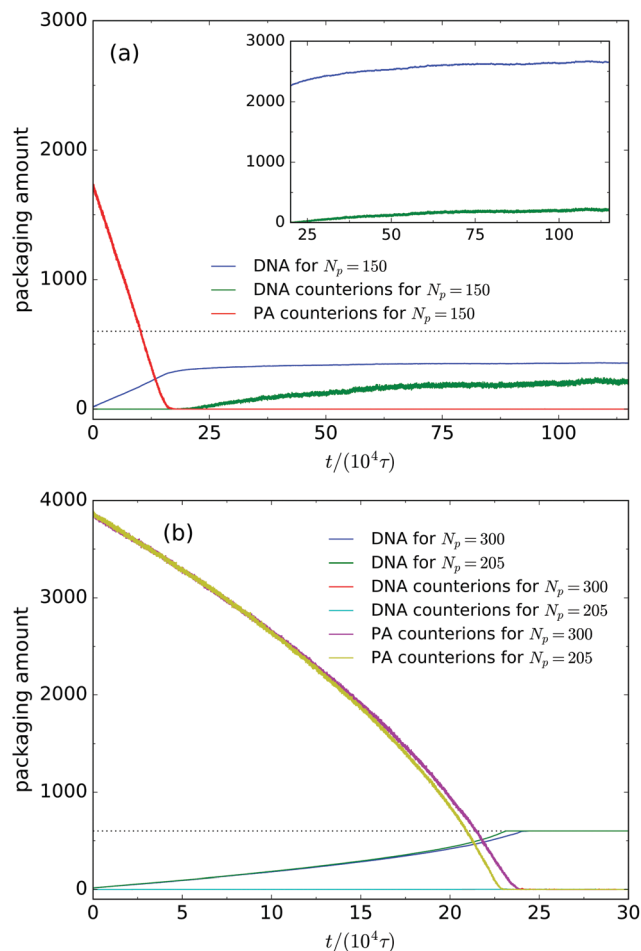


Fig. 7 Radius of gyration  $R_g$  of the PA chains as a function of the number of the PA chains. Two chain lengths,  $N_{pm} = 30$  and 44, are studied. In all cases, the entire DNA chain is packed into the capsid. At high grafting densities, no motor force is exerted to assist the DNA intrusion. At low grafting densities, a force of  $100f^*$  is applied to the DNA beads in the opening region.

at high grafting densities.  $R_g$  is insensitive to  $N_p$  regardless of the PA length. In our recent studies of charged polymer (polyelectrolyte and polyampholyte) brushes grafted on the surface of a spherical cavity, we found that the increase of the grafting density leads to a slightly smaller system size.<sup>32</sup> The concave geometry results in a higher charge density near the center of the spherical cavity and thus stronger electrostatic repulsion, compared to planar polyelectrolyte brushes. For the present system, the DNA-PA electrostatic interaction screens the PA-PA repulsion to some extent and weakening further the dependence on the grafting density.

We have also studied the packaging amount of DNA and counterions in the absence of motor force. For sparse PA layer [Fig. 8(a)], a long simulation is necessary to reach the equilibrium state. It is clear that the DNA counterions enter the capsid at a slower rate after all PA counterions are dissociated from the PAs. Once all PA counterions are expelled from the capsid, which also means the negative charges of the packed DNA are balanced by the positive charges in the PA layer, the electrostatic force that helps driving the DNA into the capsid becomes weak. The weak interaction between DNA and PAs further promotes the packaging process until the equilibrium state is reached. Simultaneously, the excess DNA charges not compensated by the PAs induce DNA counterions to enter the capsid. Additionally, as shown in the inset of Fig. 8(a), DNA charges and their counterions enter the capsid synchronously. Fig. 8(b) also shows the packaging amount for a denser PA layer. After completion of the DNA packaging, all PA counterions are pushed out of the capsid and the DNA counterions that are adsorbed into the capsid are negligible. Therefore, the complex in the capsid is only formed by DNA and PAs. Additionally, the release rate of PA counterions keeps pace with the packaging of DNA charges.

We now discuss the contribution of electrostatic energies between different charged components. As shown in Fig. 9,



**Fig. 8** Time evolution of the packaging amount for the DNA chain and counterions in the absence of motor force. The PA length in (a) is  $N_{pm} = 30$ . The inset shows the packaging amount of the DNA charges and counterions as a function of time. In (b), the total number of charged PA units for  $N_p = 300$  ( $N_{pm} = 30$ ) is approximately equal to that for 205 (44).

the electrostatic energy  $E_e$  of the system exhibits a slow reduction during the packaging process regardless of presence or absence of the motor force. However, there is a significant change for different components of electrostatic energy. At  $N_p = 150$  [Fig. 9(a)], the electrostatic energy  $E_e^{di}$  between DNA and corresponding counterions increases until the charges of the PA layer are offset by that of packed DNA. The increase is related to the dissociation of counterions from the DNA. This process is not observed in Fig. 2, because the DNA counterions are dissociated before the DNA enters the capsid. After that, the energy decreases in correspondence with the accumulation of DNA counterions in the capsid. In the initial packaging stage, the driving force does not originate from the decrease of total electrostatic energy, while the strong binding ability between DNA and PAs is supportive of packaging. Despite the absence of motor force, a part of DNA can also be packed into the capsid spontaneously. Undoubtedly, the motor can accelerate the packaging process, and it is the main driving force at later stages.<sup>23</sup> If the amount of net charges in the PA layer is sufficiently high, the DNA chain can be pulled into the capsid

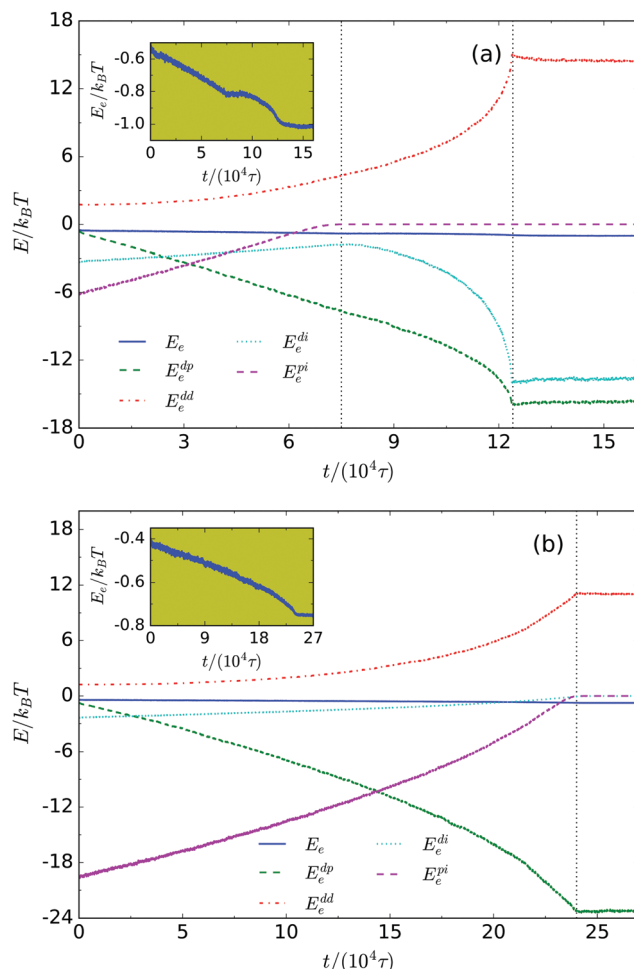


**Fig. 9** Electrostatic energy as a function of simulation time for (a)  $N_p = 150$  with motor force  $f = 100 f^*$ , and (b)  $N_p = 300$  without motor force. The PA length is  $N_{pm} = 30$ . The subscripts e, d, p and i denote the entire system, DNA, PA, and corresponding counterions, respectively. The inset shows a zoom-in view of  $E_e$ . In (a), the vertical lines from left to right represent the position where the amount of packed DNA charges is equal to that of total charges of the PA layer, and the position where the DNA packaging finishes. These two positions coincide in (b).

despite the absence of a molecular motor. As shown in Fig. 9(b), the electrostatic energy  $E_e^{dp}$  decreases spontaneously until the packaging ends. However, such condition cannot be satisfied for most viruses (see Table 1 in ref. 10). The electrostatic self-repulsion energy  $E_e^{dd}$  of the packed DNA at  $N_p = 150$  with motor force is about  $14.5 k_B T$ , which is larger than in the case of  $N_p = 300$  in the absence of motor force,  $E_e^{dd} = 11 k_B T$ . For the latter, the DNA chain adopts a more compact conformation near the capsid surface or its average bending angle is smaller than the former (the comparison is not shown here).

## Conclusion

In conclusion, based on a coarse-grained DNA and viral capsid model, we have investigated the packaging dynamics of DNA into the capsid. Unlike previous studies, counterions and peptide arms (PAs) extending into the interior of the capsid are explicitly

included in our model. During the packaging process, we observe a dynamic release or accumulation of counterions inside and outside the capsid, which cannot be captured by a model based on the simple Debye–Hückel approximation. Regarding conformational properties, we find that the packed conformation and density distribution of DNA show a significant dependence on the PA length. The packaging rate, however, is very weakly influenced. The initial packaging rate is insensitive to the total amount of PA charges in the absence of motor force. By calculating the electrostatic energy in the cases with or without motor, it turned out that the electrostatic energy of the system decreases very slowly during the entire packaging process compared to different components of the electrostatic energy. It implies that the attraction between the DNA and PA chains is the main driving force when the packaging proceeds spontaneously (*i.e.*, if no motor is present or during the initial period of DNA inclusion).

## Acknowledgements

This work has been supported by the NSF under Grant No. DMR-1463241, National Natural Science Foundation of China under Grant No. 31500801, and CNPq (National Council for Scientific and Technological Development, Brazil) under Grant No. 402091/2012-4. QC gratefully acknowledges support by the Alexander von Humboldt Foundation.

## References

- 1 D. E. Smith, S. J. Tans, S. B. Smith, S. Grimes, D. L. Anderson and C. Bustamante, *Nature*, 2001, **413**, 748.
- 2 J. Kindt, S. Tzlil, A. Ben-Shaul and W. M. Gelbart, *Proc. Natl. Acad. Sci. U. S. A.*, 2001, **98**, 13671.
- 3 W. M. Gelbart and C. M. Knobler, *Science*, 2009, **323**, 1682.
- 4 S. C. Harvey, A. S. Petrov, B. Devkota and M. B. Boz, *Phys. Chem. Chem. Phys.*, 2009, **11**, 10553.
- 5 J. A. Speir and J. E. Johnson, *Curr. Opin. Struct. Biol.*, 2012, **22**, 65.
- 6 M. E. Cerritelli, N. Q. Cheng, A. H. Rosenberg, C. E. McPherson, F. P. Booy and A. C. Steven, *Cell*, 1997, **91**, 271.
- 7 N. V. Hud and K. H. Downing, *Proc. Natl. Acad. Sci. U. S. A.*, 2001, **98**, 14925.
- 8 D. N. Fuller, J. P. Rickgauer, P. J. Jardine, S. Grimes, D. L. Anderson and D. E. Smith, *Proc. Natl. Acad. Sci. U. S. A.*, 2007, **104**, 11245.
- 9 D. Marenduzzo, C. Micheletti, E. Orlandini and D. W. Sumners, *Proc. Natl. Acad. Sci. U. S. A.*, 2013, **110**, 20081.
- 10 V. A. Belyi and M. Muthukumar, *Proc. Natl. Acad. Sci. U. S. A.*, 2006, **103**, 17174.
- 11 C. L. Ting, J. Wu and Z.-G. Wang, *Proc. Natl. Acad. Sci. U. S. A.*, 2011, **108**, 16986.
- 12 I. Ali, D. Marenduzzo and J. M. Yeomans, *Phys. Rev. Lett.*, 2006, **96**, 208102.
- 13 C. Forrey and M. Muthukumar, *Biophys. J.*, 2006, **91**, 25.
- 14 A. S. Petrov and S. C. Harvey, *Structure*, 2007, **15**, 21.
- 15 J. Arsuaga, M. Vázquez, S. Trigueros, D. W. Sumners and J. Roca, *Proc. Natl. Acad. Sci. U. S. A.*, 2002, **99**, 5373.
- 16 A. Matsuyama, M. Yano and A. Matsuda, *J. Chem. Phys.*, 2009, **131**, 105104.
- 17 O. M. Elrad and M. F. Hagan, *Phys. Biol.*, 2010, **7**, 045003.
- 18 D. G. Angelescu, R. Bruinsma and P. Linse, *Phys. Rev. E: Stat., Nonlinear, Soft Matter Phys.*, 2006, **73**, 041921.
- 19 I. Ali and D. Marenduzzo, *J. Chem. Phys.*, 2011, **135**, 095101.
- 20 N. Stoop, J. Najafi, F. K. Wittel, M. Habibi and H. J. Herrmann, *Phys. Rev. Lett.*, 2011, **106**, 214102.
- 21 J. D. Perlmutter, C. Qiao and M. F. Hagan, *eLife*, 2013, **2**, e00632.
- 22 A. D. Migliori, N. Keller, T. I. Alam, M. Mahalingam, V. B. Rao, G. Arya and D. E. Smith, *Nat. Commun.*, 2014, **5**, 4173.
- 23 Q. Cao and M. Bachmann, *J. Polym. Sci., Part B: Polym. Phys.*, 2016, **54**, 1054.
- 24 P. L. Freddolino, A. S. Arkhipov, S. B. Larson, A. McPherson and K. Schulten, *Structure*, 2006, **14**, 437.
- 25 D. Marenduzzo, E. Orlandini, A. Stasiak, D. W. Sumners, L. Tubiana and C. Micheletti, *Proc. Natl. Acad. Sci. U. S. A.*, 2009, **106**, 22269.
- 26 Q. Cao and M. Bachmann, *Phys. Rev. E: Stat., Nonlinear, Soft Matter Phys.*, 2014, **90**, 060601(R).
- 27 A. Wynveen and C. N. Likos, *Soft Matter*, 2010, **6**, 163.
- 28 C. Forrey and M. Muthukumar, *J. Chem. Phys.*, 2009, **131**, 105101.
- 29 R. W. Hockney and J. W. Eastwood, *Computer Simulation Using Particles*, Adam Hilger, Bristol, 1988.
- 30 S. Plimpton, *J. Comput. Phys.*, 1995, **117**, 1.
- 31 D. A. Goldfeld and A. Cacciuto, *Macromolecules*, 2009, **42**, 4874.
- 32 Q. Cao and H. You, *Langmuir*, 2015, **31**, 6375.
- 33 I. Ali, D. Marenduzzo and J. M. Yeomans, *J. Chem. Phys.*, 2004, **121**, 8635.
- 34 A. S. Petrov, K. Lim-Hing and S. C. Harvey, *Structure*, 2007, **15**, 807.